Effects of Microcompounding Process Parameters on the Properties of ABS/Polyamide-6 Blends Based Nanocomposites

Güralp Özkoç,[1]* Göknur Bayram,[2] Martin Quaedflieg[3]

[1]*Department of Polymer Science and Technology, Middle East Technical University, 06531 Ankara, Turkey*
[2]*Department of Chemical Engineering, Middle East Technical University, 06531 Ankara, Turkey*
[3]*DSM Xplore, P.O. Box 18, 6160 MD, Geleen, The Netherlands*

Received 1 March 2007; accepted 22 September 2007
DOI 10.1002/app.27460
Published online 26 November 2007 in Wiley InterScience (www.interscience.wiley.com).

ABSTRACT: Melt intercalation method was applied to produce acrylonitrile-butadiene-styrene/polyamide-6 (ABS/PA6) blends based organoclay nanocomposites using a conical twin-screw microcompounder. The blend was compatibilized using a maleated olefinic copolymer. The effects of microcompounding conditions such as screw speed, screw rotation-mode (co- or counter-), and material parameters such as blend composition and clay loading level on the morphology of the blends, dispersibility of nanoparticles, and mechanical properties were investigated. Furthermore, corotating screws were modified to achieve elongational flow which is efficient for obtaining dispersive mixing. The morphology was examined by SEM analysis after preferential extraction of the minor phase. Subsequently, the SEM micrographs were quantitatively analyzed using image analyzer software. The morphology of the blends indicated that processing with counter-rotation at a given screw speed yielded coarser morphology than that of processed with corotation. X-ray diffraction analysis showed that highest level of exfoliation is observed with increasing PA6 content, at 200 rpm of screw speed and in corotation mode. Also, the effects of screw speed, screw rotation mode, and screw modification were discussed in terms of XRD responses of the nanocomposites. The aspect ratio of the clay particles which were measured by performing image analysis on TEM micrographs exhibited a variation with processing conditions and they are in accordance with the modulus of the nanocomposites. © 2007 Wiley Periodicals, Inc. J Appl Polym Sci 107: 3058–3070, 2008

Key words: nanocomposites; blends; compounding; ABS; polyamide-6

INTRODUCTION

Organically modified layered silicate nanocomposite materials have attracted both scientific and industrial interest after the introduction of melt intercalation method to produce nanocomposites by Vaia et al.,[1,2] because they exhibit improved physical properties such as modulus, tensile strength, heat distortion temperature, and barrier properties at very low filler loadings. Extrusion compounding is the most common method to produce intercalated or exfoliated nanocomposites. Therefore, several studies has been conducted to understand the influence of extrusion parameters such as type of the processing device (i.e. single screw extruder, co- or counter rotating twin screw extruder), processing conditions (i.e. screw speed, barrel temperature, and mixing order) which affect the state of dispersion of nanofillers.[3–6]

Laboratory-scale mixing devices, which serve as cost and time efficient research facilities, provide possibilities of processing a few grams of material and they have the capability of continuous or batch processing with the same thermal environment as a conventional extruder.[7,8] Microdevices can be used as fast screening tools in the field of polymer based nanocomposite development.[7–13] There are few number of studies focused on the design and mixing behavior of these small scale mixing devices. Walia et al. compared the mixing efficiency of a batch mixer and minicompounder during preparation of poly(methyl methacrylate)/polystyrene blends.[10] They reported that from distributive mixing point of view, the microcompounder mixed similarly to the batch mixer under moderate mixing conditions, on the other hand the microcompounder performed less favorably compared to the batch mixer under vigorous mixing conditions. Maric and Macosko investigated the mixing ability of the laboratory mixing devices (i.e. batch mixer, twin screw mini compounder, a lab-scale conventional twin screw extruder, and a mini mixer mixing with the help of

**Present address:* Kocaeli Üniversitesi Mühendislik Fakültesi Veziroğlu Yerleşkesi, Eski Gölcük Yolu 41040 İzmit/Kocaeli, Turkey.
Correspondence to: G. Özkoç (guralp.ozkoc@kou.edu.tr).
Contract grant sponsors: DSM Xplore, Turkish State Planning Organization through Faculty Development Program (OYP) of Middle East Technical University.

steel balls) in polystyrene/poly(dimethyl siloxane) blends.[14] It was concluded in their study that the twin screw extruder resulted in the finest particle size among the mixers. The other mixing equipments lead to similar particle sizes. Breuer et al. designed and tested a new miniature mixer especially for polymer blends and nanocomposites.[15] Their new mixing device has a capacity of $\sim$ 2 g of material. The mixer has an asymmetrically designed rotor and it was claimed to support complex flow modes providing dispersive mixing. The tests conducted by the authors showed that small dispersed phase size of polypropylene/polyamide and polystyrene/polypropylene immiscible blends was superior to the other mixing devices. Nanocomposites prepared in this new miniature extruder exhibited well-distribution under high shear conditions. Covas and Costa[16] developed a miniature extrusion line for small scale processing studies to produce extrudates using few grams of raw polymer. The extruder consisted of a vertical single screw (L/D: 11.5) which can be operated in continuous mode to obtain a constant cross-section of product. They also tried to improve the mixing efficiency of the extruder using specially designed elements on the screw. The result of the study pointed out that the dispersive capacity of the extruder with mixing element is similar to that of a corotating extruder.

In the current study, a conical mini twin screw extruder (microcompounder, hereafter) with a recirculation facility was utilized as the processing device for the production of nanocomposites. Beyond the advantages of this device (i.e. cost and time efficient processing), there appear also some potential disadvantages. Completely flighted screws are not equipped with mixing elements, and consequently can not create complex flow types which are more efficient in dispersive mixing. As a result of similar geometrical design of two screws, the melt conveying characteristics are analogous to each other; therefore, despite twin screws, the flow type of the melt of extruder is similar to that of a single screw extruder without having any mixing elements.[17,18] Hence, it lacks some advantages of twin screw extruders such as elongational flow promoting dispersive mixing.

This article concentrates on the effects of microcompounding process conditions such as screw speed, screw rotation-mode (i.e. co- or counter-rotation), and mixing time as a function of blend composition and clay loading in acrylonitrile-butadiene-styrene terpolymer/polyamide-6 (ABS/PA6) blends based organoclay nanocomposites. ABS/PA6 blends are of significant commercial interest, because they exhibit good balance of toughness and stiffness. Because of the presence of highly polar end groups of PA6, the simple blends of ABS and PA6 are incompatible; therefore it is necessary to compatibilize these materials to achieve improved properties. Therefore, several researchers have focused on the compatibilization of PA6 and ABS.[19–25] The studies conducted in our laboratory showed that olefin based functional copolymers such as CO modified ethylene-*n*-butyl acrylate-maleic anhydride or ethylene-methyl acrylate-glycidyl methacrylate are potential compatibilizer yielding a fine blend morphology with enhanced mechanical properties.[26,27] Thus, in the current study CO modified maleated ethylene-*n*-butyl acrylate copolymer was selected as a compatibilizer.

Furthermore, it was also aimed to modify the currently available corotating screws by machining narrow channels (2-mm wide) through screw flights slots [see Fig. 1(c)] and test in terms of blend morphologies, nanoparticle dispersion and mechanical property enhancement. It was shown in the literature that such kind of channels enforces the polymer melt to flow through this channel, and consequently polymer melt is exposed to an elongational deformation.[28–30]

MATERIALS AND METHODS

Materials

The materials used in this study are specified in Table I. Prior to compounding, ABS and PA6 pellets were dried in a vacuum oven at 80°C for 12 h, carbonmonoxide modified ethylene-*n*-butyl acrylate-maleic anhydride (EnBACO-MAH) was dried at 50°C for 4 h under vacuum. The organoclay was methyl tallow bis-2-hydroxyethyl quaternary ammonium modified montmorillonite (MMT). The ABS/PA6 ratio chosen were 0/100, 20/80, 50/50, 80/20, and 100/0. The percentage of (ABS+PA6) portion of the matrix was 95% and compatibilizer was 5% of the matrix (blends will be named in the order of ABS/PA6/Compatibilizer by giving the ratios, hereafter). MMT amount was varied as 1, 3, and 5% by weight of the nanocomposites.

Microcompounding and injection molding

First, (ABS/PA6)/Compatibilizer batches at predetermined compositions were dry-mixed at predefined amounts with a precision of 0.01 g. The mixture was melt compounded in a twin-screw microextruder (15-mL microcompounder®, DSM Xplore, Geleen, The Netherlands). Figure 1 shows the cross-section of the barrel of this laboratory extruder in corotating, counter rotating, and modified corotating modes. The core of this laboratory compounder is formed by a separable, sealed mixing compartment containing two detachable, conical mixing screws. The main drive is continually digitally variable and allows for torque measurement. The processing tem-

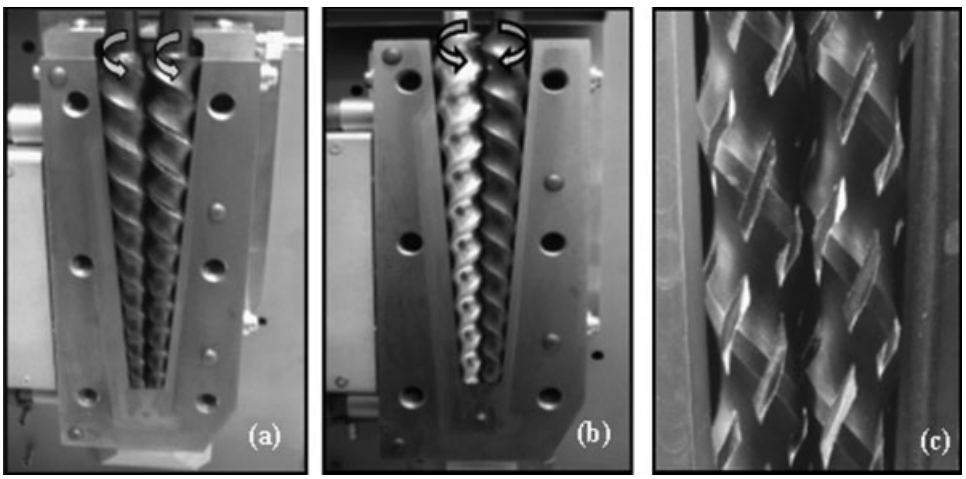

Figure 1 The cross-sections of (a) corotating, (b) counter-rotating, and (c) modified corotating screw.

perature can be adjusted in three separately controlled heating zones and the mixing time can be varied via recirculation of the melt. This laboratory extruder can be operated in both corotating and counter-rotating mode by the help of a gear box fixed on the main drive of the machine.

Materials were fed from the top of the microextruder by a specially designed injector type feeder. The screw speed was kept at 30 rpm during feeding. Feeding took about 15 s. After feeding, the screw speed was increased to operating value. The operating conditions of the microextruder were arranged as screw speeds of 100 and 200 rpm and barrel temperature profile of 235-235-235°C (from top to bottom). The mixing time was kept constant at 3 min. At the end of this period, the extrudate was taken by changing the position of the valve to guide the polymer to the die.

Materials were injection molded using a DSM Xplore 10-mL injection molding machine® to obtain ISO 527-2/5A tensile bars. The injection and holding pressures were set to 15 bars. Melt temperature and mold temperature were 235 and 80°C, respectively.

X-ray analysis

X-ray analysis was conducted using narrow part of injection molded tensile bars for nanocomposites by using a RIGAKU D/MAX 2200/PC X-ray diffractometer using X-ray source of Cu Kα (λ = 1.54Å) radiation generated at a voltage of 40 kV and current of 40 mA. The diffraction angle 2θ was scanned from 1° to 10° at a scanning rate of 1°/min. Organoclay was analyzed in powder form under same conditions. The XRD patterns were used to calculate final *d*-spacing of the clay galleries by using Bragg's Law.

Tensile testing

Prior to testing, the tensile bars were kept in a desiccator in polyethylene bags for at least 24 h. Tensile test were performed on dog-bone shaped samples according to ISO 527-2 using tensile testing machine (Instron Model 1137) at 23°C. The crosshead speed was 2.5 mm/min. For each experiment, 5 samples were tested. The average results were reported with standard errors.

TABLE I
Specifications of the Materials Used in the Study

Material	Trade name and supplier	Specifications
ABS	Lustran ABS M203FC, Lanxess	Density: 1.05 g/cm^3 MFI (220°C and 10 kg): 32.5 g/10 min Standard impact strength, easy flowing
PA6	Teklamid 6, Polyone	Density: 1.13 g/cm^3 MFI (235°C and 2.16 kg): 34.25 g/10 min Natural, unfilled, extrusion grade
EnBACO-MAH	Fusabond A MG423D, Dupont	MFI (190°C, 2.16 kg): 8 g/10 min Melting point: 62°C MAH content ~ 1 wt %
Montmorillonite (MMT)	Cloisite® 30B, Southern clay products	Organic modifier: Methyl, tallow, bis-2-hydroxyethyl, quaternary ammonium Density: 1.98 g/cm^3 *d*-spacing = 18.5Å

Scanning electron microscopy

The cryogenically fractured surfaces of injection molded samples were analyzed by using a low voltage SEM (JEOL JSM-6400) to observe the morphology of the nanocomposites. PA6 and ABS phases were etched by immersing the fracture surfaces in formic acid for 15 min and in THF for 60 min, respectively, to observe the blend phase morphologies. To prevent arcing, sample surfaces were coated with gold. To calculate the apparent dispersed particle diameters, the areas of the particles were measured automatically using image analyzer software (Image J 1.36, USA), then apparent diameters, d_{app}, were calculated using eq. (1) by assuming globular particles:

$$d_{app} = 2(A/\pi)^{1/2} \quad (1)$$

where A is the area of the particle analyzed which was obtained as an output using software. The distribution of d_{app} was obtained by measuring at least 300 particles. The average apparent diameters, $(d_{app})_{avg}$, were calculated using eq. (2):

$$(d_{app})_{avg} = (\Sigma_{n_i d_i})/(\Sigma_{n_i}) \quad (2)$$

where n is the number of the particle with apparent diameter size, d.

Transmission electron microscopy

Injection molded samples were examined by Transmission Electron Microscope (Philips CM200 TEM) at an acceleration voltage of 120 kV. Ultra thin sections of 70 nm thickness were cryogenically cut with a diamond knife at a temperature of -100°C. All samples were trimmed parallel to the injection molding direction.

The resulting images were analyzed to observe the extent of exfoliation and to obtain particle size distribution. Because of the slight variation in the thickness of the ultra-microtomed section, grey shades appeared on the TEM micrographs and they disturb the clearness of the image and reduce the image quality for the analysis. To make the clay layers, stacks and tactoids much clear and visible,[31] selected TEM micrographs (at same magnification) were printed on A4-size papers at photographic quality by using a laser-printer. Then, the particles were traced on transparency films with a permanent pen. The resulting transparencies were scanned at 300 dpi resolution on a white background to obtain maximum contrast for image analysis. The scanned images were analyzed using an image analyzer for automatic particle size distribution using an image analyzer (Scion Image, USA). At least 250 particles were analyzed for each composition. The average particle lengths, l_{avg}, were calculated using eq. (3):

$$l_{avg} = (\Sigma_{n_i l_i})/(\Sigma_{n_i}) \quad (3)$$

where n is the number of the particle with length, l.

To obtain the average particle thickness, the number of platelets/particle was counted and marked manually on the print-out of the TEM micrographs. The average number of platelets/particle, n_{avg}, was calculated using eq. (3) by taking number of platelets/particle (n) instead of particle length (l). The details of calculation of average particle thickness are mentioned in the following part.

RESULTS AND DISCUSSION

Blend morphologies by SEM analysis

One of the important issues affecting the performance of the blends is the blend morphology. For multicomponent polymer systems, the morphology of the phases is controlled by droplet break-up process.[32,33] The parameters that influence this process are given by the capillary number, Ca, which is the ratio of the deforming stress to the interfacial forces[34]:

$$Ca = \frac{\eta_m \dot{\gamma}}{\sigma/R} \quad (4)$$

where η_m is the matrix viscosity, $\dot{\gamma}$ is the shear rate in simple shear flow, σ is the interfacial tension, and R is the droplet radius. If Ca is higher than a critical value, Ca_{crit} the particle becomes unstable and breaks-up. To have larger Ca, either a high $\dot{\gamma}$ or small σ should be required for a given polymer couple. In the current study, the matrix viscosity η_m and σ are kept constant by fixing the composition of the ABS/PA6/Compatibilizer blends. Therefore, only parameter is the shear rate, $\dot{\gamma}$, imposed by the flow in the extrusion.

The SEM micrographs of 80/20/5 blend system processed at 100 rpm are shown in Figure 2(a,b) as a function of screw rotation mode. The black holes seen in micrographs are left after removal of PA6 phase by etching. It is seen that, the particle size of PA6 in corotation is much finer than that of in counter-rotation (1.72 and 6.30 μm, respectively). This variation in phase sizes can be attributed to the insufficient shear rate in counter rotation mode under same processing conditions.[35] Another factor is the flow patterns of the polymer melts. In tightly intermeshing counter-rotating extruders, the screw-speeds in the intermeshing region are in the same direction; therefore material which enters the intermeshing section continues to flow through this region. However, when the clearance between the screws is very small, the amount of

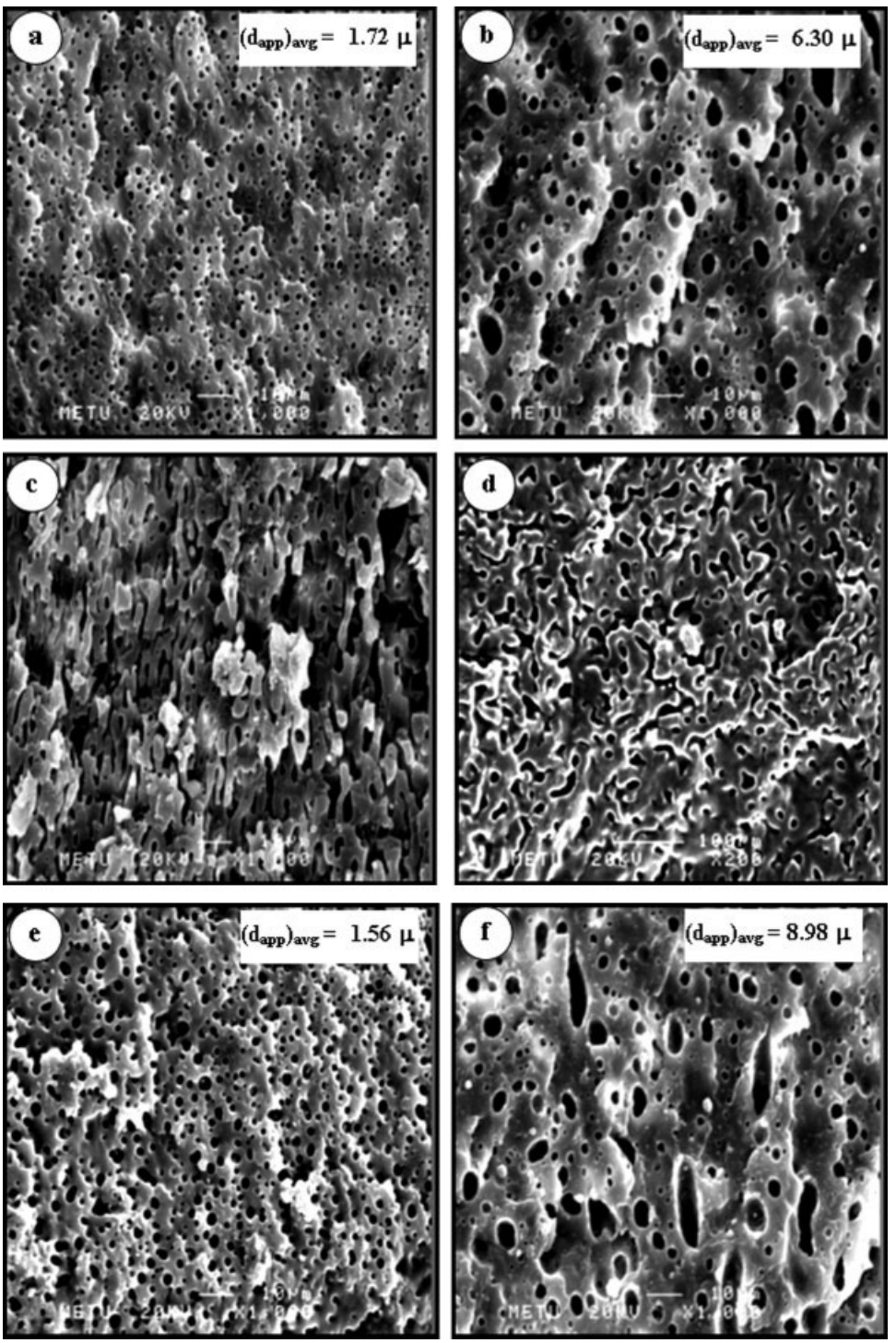

Figure 2 SEM micrographs of (a) 80/20/5 processed with corotating twin screws at 100 rpm (×1000), (b) 80/20/5 processed with counter-rotating twin screws at 100 rpm (×1000), (c) 50/50/5 processed with corotating twin screws at 100 rpm (×1000), (d) 50/50/5 processed with counter-rotating twin screws at 100 rpm (×200), (e) 20/80/5 processed with corotating twin screws at 100 rpm (×1000), (f) 20/80/5 processed with counter-rotating twin screws at 100 rpm (×1000).

material which can flow through the intermeshing region will be quite small. As a consequence, a mass of material starts to accumulate at the entry of this region.[18] This accumulation can lead to coalescence of the dispersed phase which results in larger dispersed particles.

When the blend ratio is changed to 50/50/5 [see Fig. 2(c,d), black holes seen in micrographs are left after removal of PA6 phase by etching], the dispersed phase morphology is altered to cocontinuous morphology.[26,27] In corotation, this variation in morphology is more significant than in counter-rotation.

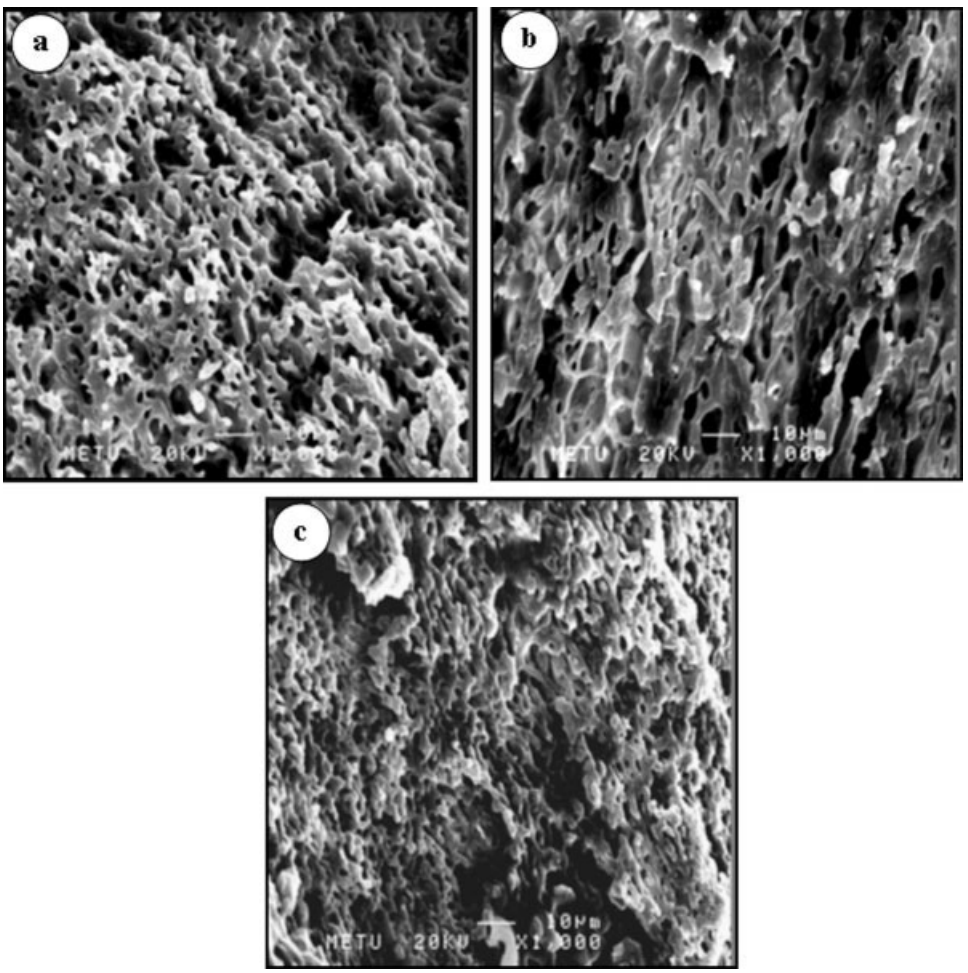

Figure 3 SEM micrographs of 50/50/5 blend based nanocomposites containing 5 wt % clay (a) processed with corotating twin screws at 100 rpm, (b) processed with counter-rotating twin screws at 100 rpm, (c) processed with modified corotating twin screws at 100 rpm.

In counter-rotation, a combination of cocontinuous and very coarse, nonspherical dispersed phase morphology is observed.

Further increase in PA6 to ABS ratio resulted in dispersed phase morphology, but in this case PA6 is the continuous phase and ABS is the dispersed phase [see Fig. 2(e,f), black holes seen in micrographs are left after removal of ABS phase by etching]. Image analysis results indicate that in corotation the average dispersed phase size is smaller than that in counter-rotation.

The effect of the screw rotation-mode and modification on the morphology of 50/50/5 blend based 5% clay containing nanocomposite are shown in Figure 3(a–c). The black holes seen in micrographs are left after removal of ABS phase by etching. Regardless of processing history, all the three cases are cocontinuous. However, the level of capillarity of the phases is different in all cases. In modified corotation, the phases are more entangled in each others than the ones in counter and corotation.

Observations on dispersion of nanoparticles by XRD and TEM

Figure 4 displays the XRD curves of 5 wt % organoclay containing nanocomposites based on ABS, PA6 and their compatibilized blends as the function of processing conditions and blend composition. The curve (1) in Figure 4(a–d) is the XRD pattern for Cloisite 30B showing an intense, broad peak at $2\Theta = 5.0^\circ$, corresponding to a basal spacing (d_{001}) of 18.0 Å. The nanocomposite based on pure PA6 [0/100 in Fig. 4(a)] does not exhibit any peak relevant to clay layers. This can be considered as fully exfoliated structure. On the other hand, the nanocomposite based on ABS [100/0 in Fig. 4(a)] exhibits a sharp peak at $2\Theta = 2.44^\circ$ corresponding to a basal spacing of 36.18 Å and a broad peak around $2\Theta = 5.0^\circ$. This implies that most of the clays are intercalated but there still exists some unexfoliated stacks.[36]

XRD curves of 80/20 blend based nanocomposites prepared at different processing conditions are given in Figure 4(b). The addition of PA6 into the ABS to-

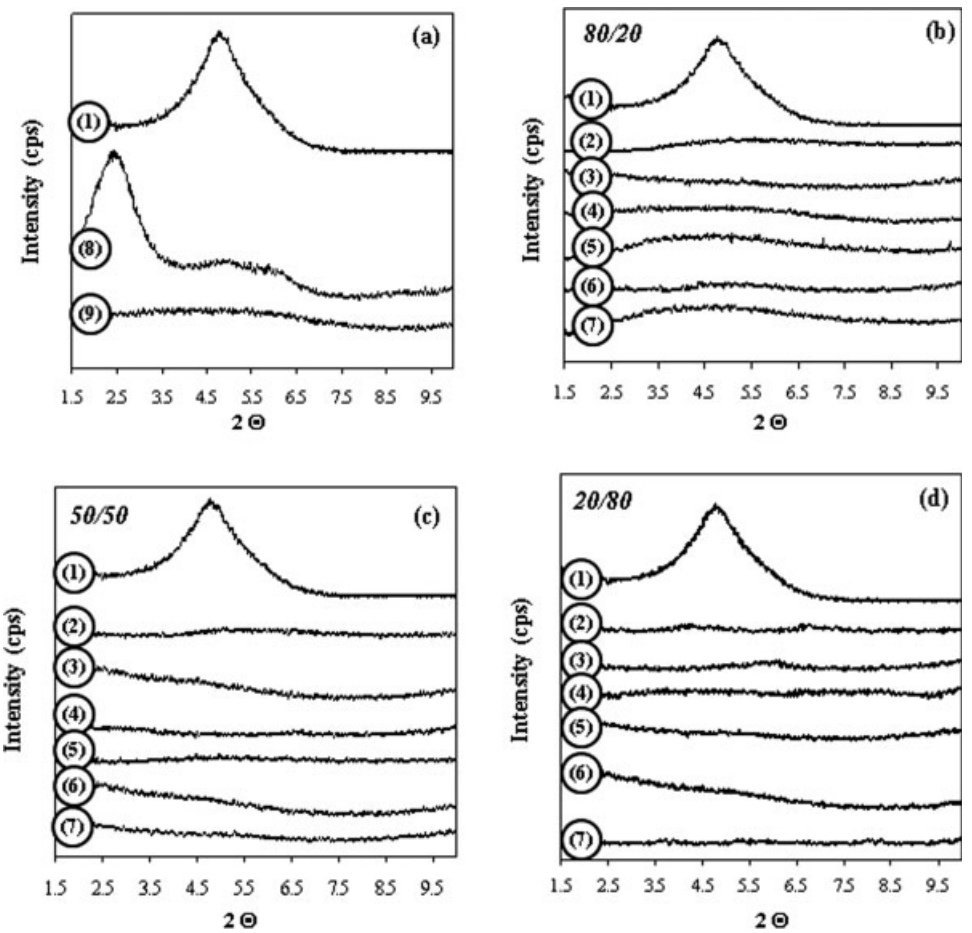

Figure 4 XRD patterns of nanocomposites containing 5 wt % organoclay based on (a) pure matrices, (b) 80/20 blend, (c) 50/50 blend, (d) 20/80 blend. [The numbers stand for (1) Cloisite® 30B, (2) 200 rpm modified corotation, (3) 100 rpm modified corotation, (4) 200 rpm counter-rotation, (5) 100 rpm counter-rotation, (6) 200 rpm corotation, (7) 100 rpm corotation, (8) ABS based nanocomposites, 100 rpm corotation, (9) PA6 based nanocomposites, 100 rpm corotation (XRD patterns were vertically offset for clarity)].

gether with a compatibilizer resulted in a very broad peak [see Fig. 4(b) (7)]. This means that most of the clays are exfoliated; however there still exist unexfoliated or intercalated platelets, so called stacks. One should note that the organoclay, Cloisite 30B, used in the current study is confirmed to be compatible with PA6 in PA6/organoclay and PA6-polymer blends/organoclay nanocomposites.[37–40] Therefore, increase in level of exfoliation by the incorporation of PA6 can be attributed to improved compatibility between the organoclay and polymer matrix. Doubling the screw-speed to 200 rpm increased the level of exfoliation, therefore no peak is observed for curve (6). When counter-rotation is considered (curves 4 and 5), the broad peak at 100 rpm (curve 5) disappears as the screw speed is increased to 200 rpm. XRD patterns of the nanocomposites prepared using modified screw (curves 2 and 3) do not exhibit any peak relevant to organoclay pointing a fully exfoliated dispersion of organoclay platelets. In contrast, organoclay peaks are fully absent in all XRD curves of 50/50 and 20/80 blends based nanocomposites independent of processing history as the PA6 ratio is increased. Thus, it can be expected that morphology of nanocomposites based on 50/50 and 20/80 blends prepared at different processing conditions contains a substantial amount of individual platelets dispersed in the matrix. XRD results suggest that the chemical affinity plays a significant role in exfoliation mechanism. When the concentration of PA6 (compatible with Cloisite 30B) is not high enough to exfoliate all the clays, processing conditions become significant as in the 80/20 blend system.

Some representative TEM micrographs of the nanocomposite systems are given in Figures 5–7. When the nanocomposite based on ABS is considered (see Fig. 5), a combination of clay stacks seen as dark spots and delaminated platelets seen as individual particles located in the outer part of the stacks are observed. This also confirms the results of

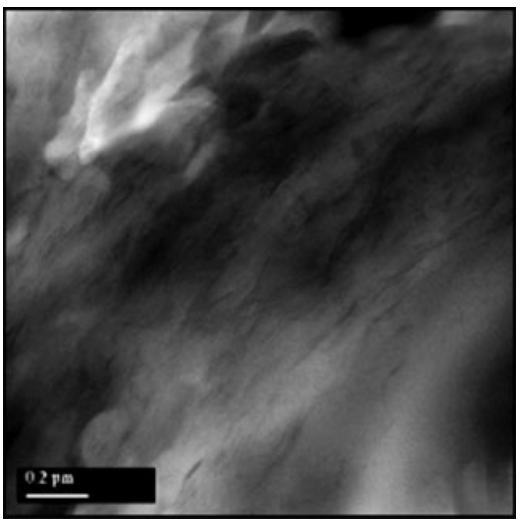

Figure 5 TEM micrograph of nanocomposite based on ABS (100/0) containing 5 wt % organoclay processed at 100 rpm corotation mode.

the XRD analysis which indicates an intercalated structure of ABS/organoclay nanocomposites. Figure 6(a,b) display TEM micrographs of the representative 50/50 blend based composites processed at 100 rpm with corotating screws. The dark region is the PA6 and the grey surrounding region is the ABS phase. Clays are selectively dispersed in PA6 phase and there is no clay platelet seen in ABS phase possibly because of the higher chemical affinity of clay to PA6 rather than ABS. Similar observation is also presented elsewhere[37,38,41,42] for PA6 blends based nanocomposites. The higher magnification in TEM image [see Fig. 6(b)] of PA6 phase shows that clay platelets are mostly exfoliated as individual layers indicating nanoscale dispersion; however few double or triple layered skewed stacks[43–45] are also observed.

The nanomorphology of the composites based on 50/50 blend processed at 100 rpm with counter-rotation or modified corotation is seen in Figures 7 and 8, respectively. Note that the selective dispersion of clay layers in PA6 is also valid for these materials but the relevant lower magnification TEM pictures are not shown here. TEM micrographs show a well-exfoliated structure consisting largely of individual clay platelets dispersed within PA6 matrix.

The white spots seen in the TEM micrographs stand for the compatibilizer domains. It is seen that the phase sizes of the compatibilizer are smaller than 0.5 μm. The compatibilizer, EnBACO-MAH, is dispersed in both ABS and PA6 phases. However, the domain sizes in ABS phase are much larger than those in PA6 phase [see Fig. 6(a)]. Clays are not dispersed in the compatibilizer domains.

To better discern between the processing conditions, a semiautomated image analysis was conducted by aiming to obtain average aspect ratio (AR_{avg}) of nanoparticles which can be considered as an indicator for the level of dispersion and defined as the average length per average thickness, $AR_{avg} = l_{avg}/t_{avg}$.

The particle thickness is obtained from the following equation[31]:

$$t_{particle} = d_{001}(n-1) + t_{platelet} \quad (5)$$

where $t_{particle}$ is the thickness of each particle, d_{001} is the spacing for the intercalated clay or organoclays, n is the number of platelet per stack (obtained manually counting from the high resolution TEM images), and $t_{platelet}$ is the thickness of each individual clay platelet. d_{001} is 1.8 nm as obtained from X-

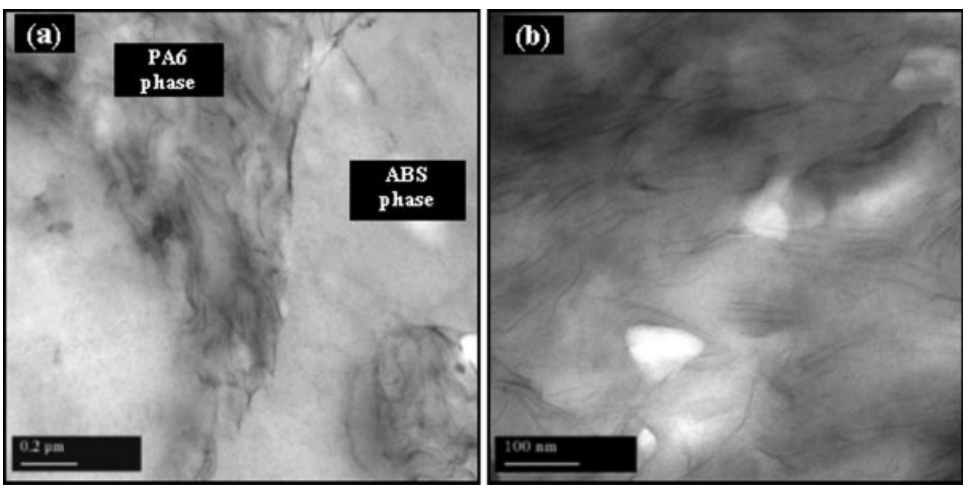

Figure 6 TEM micrographs of nanocomposite based on 50/50 blend system containing 5 wt % organoclay processed at 100 rpm in corotation mode (a) Nanomorphology of blend showing both two phases, (b) Nanomorphology of PA6 phase only.

ray analysis and $t_{platelet}$ is 0.94 nm as reported by Fornes and Paul[31] for the clay, Cloisite 30B, used in the current study. The results of image analysis and AR_{avg} calculation are summarized in Table II. It should be noted that the image analysis is performed only for the 5% clay containing 50/50 blends as a function of processing condition.

Average number of platelets per particle is less than 2 in each condition. This means that the number of exfoliated layers into single platelet is much higher than that of stacks formed by multiple platelets. Screw speed in corotation has no significant influence on the AR_{avg} (see I and II in Table II). When average length of particles (l_{avg}) and platelet per particle (n) are taken into account, increasing screw speed slightly decreased both of them in the corotation mode. The modification of the screw to promote elongational flow resulted in an improvement in AR_{avg} with respect to unmodified corotating screws regardless of screw speed (III and IV in Table II). The level of dispersion capability of counter-rotating screws was lower than that of modified or unmodified corotation when the AR_{avg} of the particles are taken into account at 100 rpm.

Axial force measurements during microcompounding

Figure 9 shows the schematic of axial force measurement set-up. The barrel of the microextruder is positioned on a lever, which swivels around a stationary axis and counter balanced by a load-cell at the other end. The load-cell is typically 10 kN in range and measures the axial force exerted by the barrel opposing the pushing forces imposed by the screws toward the bottom while the melt is pumped through the recirculation channel or die. Either the screw speed or axial force can be controlled fixing one of them by means of a control unit. This also provides the opportunity of controlling throughput in some certain applications. In the current study, the axial force measurement is conducted to verify the screw modification and to obtain qualitative information about rheological properties of nanocomposites as a function of matrix composition. All the vertical force data are obtained at the end of 2 min of mixing to ensure that there is no unmolten polymer that remained in the extruder.

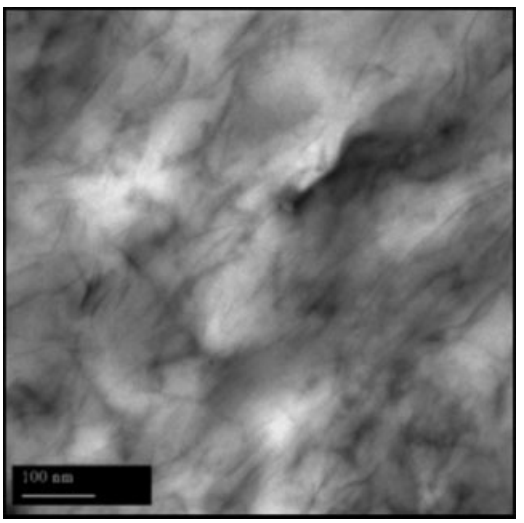

Figure 7 TEM micrographs of nanocomposite based on 50/50 blend system containing 5 wt % organoclay processed at 100 rpm in counter-rotation mode (PA6 phase).

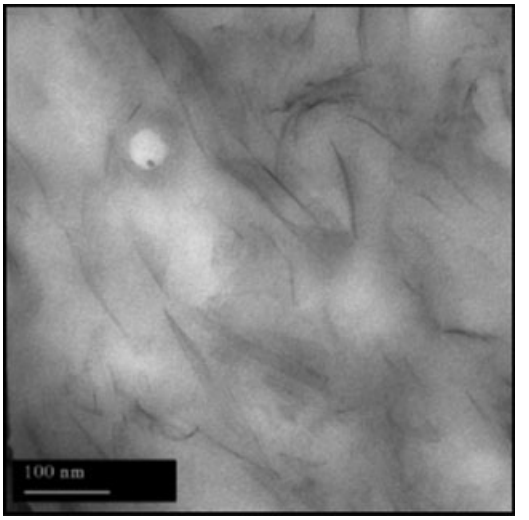

Figure 8 TEM micrographs of nanocomposite based on 50/50 blend system containing 5 wt % organoclay processed at 100 rpm in modified corotation mode (PA6 phase).

Figure 10 shows the dependence of axial force on the screw geometry, speed, and blend composition. Under the same processing conditions (i.e. screw geometry, screw speed, and barrel temperature), the axial force measured depends on the melt viscosity of the system. It can be observed from the Figure 10 that increasing PA6 in the nanocomposite decreases the axial force. This indicates that the melt viscosity of the nanocomposites is inversely proportional to the PA6 composition in the blend and directly proportional to the level of exfoliation seen in XRD plots.

The influence of addition of compatibilizer to the viscosity of the nanocomposite is only examined for 50/50 blend system. It is observed that the incorporation of compatibilizer to the blend results in an increase in the viscosity of the nanocomposite slightly at 100 rpm and significantly at 200 rpm, regardless of the screw geometry. Also note that doubling the screw speed increases the axial force, as expected.

The most important result revealed from axial force measurements is the dependence of axial force

TABLE II
Results of Image Analysis Performed on TEM Images for Selected Compositions

No	Nanocomposite system (ABS/PA6/Comp.) 5% Clay	Number of particles analyzed	Average particle length, l_{avg} (nm)	Average platelets/ particle, n	Average particle thickness, t_{avg} (nm)	Average aspect ratio (l_{avg}/t_{avg})
I	50/50/5 processed at 100 rpm	343	112.1	1.36	1.59	70.5
II	50/50/5 processed at 200 rpm	325	101.0	1.26	1.41	71.6
III	50/50/5 processed at 100 rpm with modified corotation screws	279	129.2	1.12	1.16	111.4
IV	50/50/5 processed at 200 rpm modified corotation screws	322	128.2	1.13	1.17	109.6
V	50/50/5 processed at 100 rpm counter-rotation	296	107.2	1.45	1.75	60.9

on the screw geometry for a given blend system and screw speed. As the axial forces measured at the same processing conditions and for a given blend composition are considered, the screw modification in corotation results in a lower value in comparison with unmodified one. This result indicates that more material is flowing backward due to backpressure in presence of slots on the screw flights. As a result of backflow, the melt can be subjected to elongational flow due to jetting through the channels and broader residence time distribution can be achieved in the mixing chamber. Figure 11 shows the suggested flow pattern for modified corotating screws. The polymer was separated from the screws after cooling.

The axial force values measured in counter-rotation are higher than those measured in modified corotation for all screw-speeds and all blend compositions. In comparison with corotation, significantly higher values are measured in the case of counter rotation, because of the mixing and transport characteristics of the counter rotation, which is discussed in morphology section.

Tensile properties

It has been known that modulus of composites is a function of filler volume fraction, filler aspect ratio, filler modulus, filler orientation, and interfacial adhesion. Fornes and Paul conducted theoretical studies, which were benchmarked against experimental data, to model the modulus of the PA6/organoclay nanocomposites by utilizing Halpin-Tsai theory.[31] It is pointed out in their publications that modulus of a given nanocomposite system depends on the level of dispersion of the clay platelets as a result of processing history and surface chemistry of clay. By using this approach, in the current study, the modulus of the nanocomposites is taken as an indication of level of dispersion of the platelets for a given matrix.

Figure 12 compares the responses of Young Modulus of 5% clay containing nanocomposites as the function of screw speed, screw rotation mode, and blend ratio. In the case of ABS, increasing screw speed and changing screw geometry from corotation to counter-rotation do not significantly influence the modulus of the resulting nanocomposite. The changes measured in ABS are between the error limits. When the PA6 based nanocomposites were considered, the modulus of the nanocomposites is higher in corotation than that in counter-rotation regardless of the screw speed. In either corotation or

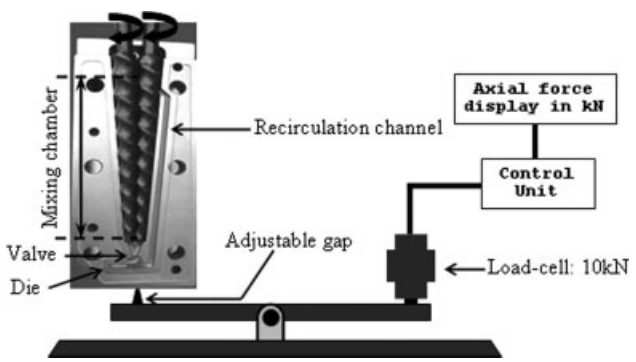

Figure 9 The schematic of axial force measurement setup.

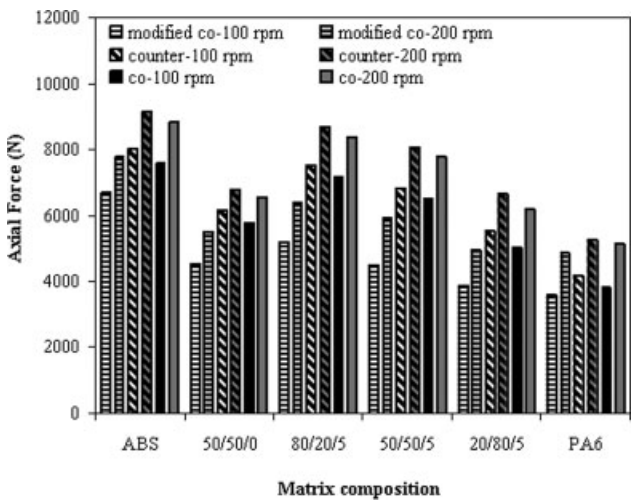

Figure 10 Dependence of axial force on screw geometry, speed and blend composition for nanocomposites containing 5 wt % organoclay.

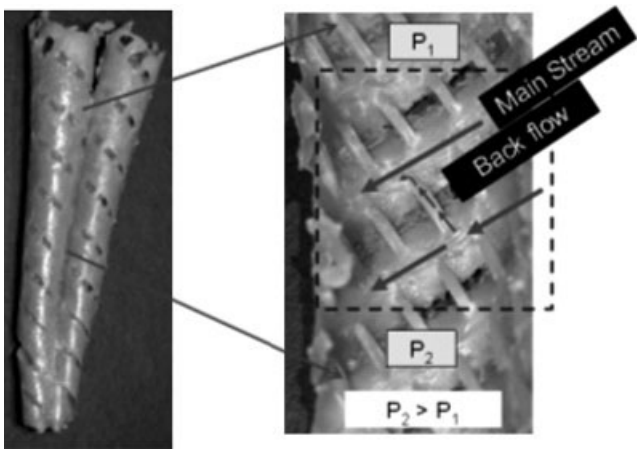

Figure 11 Schematic view of suggested flow pattern for modified corotating screws (P_1 and P_2 stands for pressure at the top and bottom, respectively).

counter rotation, doubling the screw speed results in an increase in modulus of the PA6 based nanocomposites.

The tensile modulus of the ABS/PA6 blends based nanocomposites also shows variations with processing conditions. For the 80/20 blend system, the modulus in corotation is higher than that in counter-rotation (see Fig. 12). Improved clay dispersion in PA6 phase together with much smaller diameter of the reinforced spherical PA6 phase seen in SEM micrographs are the possible reasons of obtaining higher modulus in corotation. The nanocomposites formed from 80/20/5 blend can be handled as particulate filled ABS in which clay reinforced PA6 and ABS can be considered as reinforcing filler and polymer matrix, respectively. For such systems, it was experimentally shown that the filler size is inversely proportional to the strength and stiffness of the composites.[46–48] Increasing screw speed causes an improvement in modulus of nanocomposites in corotation, however no effect is observed in counter-rotation by doubling of the screw speed.

The dependence of tensile moduli on screw rotation mode is more pronounced in nanocomposites based on 50/50/5 and 20/80/5. The moduli measured in corotation deteriorated in counter rotation at both 100 and 200 rpm. When the screw speed is doubled, a slight increase in moduli is obtained. When the moduli of the blend based nanocomposites are considered, an improvement with PA6 content is observed. Possible reason for this increase can be the dilution of the intercalated clays by the increasing PA6 concentration, which can prevent the formation of the clusters of the intercalated and/or exfoliated platelets.

Figure 13 shows the Young Modulus of 50/50/5 blend based nanocomposites as a function of screw speed, screw modification, and clay loading level. As can be seen, incorporation of organoclay improves the modulus of the blends substantially. This increasing stiffness of the final structure can be a consequence of the interaction of the polyamide, in which clays are selectively localized, and organic surfactant. This interactions lead to restriction of the mobility of the polyamide molecules. As a result, one of the components of the blend system becomes stiffer, which increase the overall modulus of the blend. Increasing clay concentration results in an increase in modulus regardless of the screw speed and screw modification.

It has been already shown that modification of the screw by inserting flight slots results in more back-

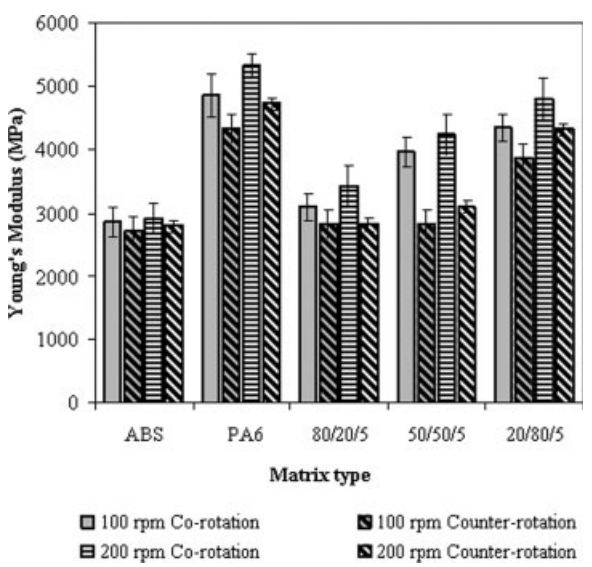

Figure 12 Young's Modulus of nanocomposites containing 5% clay as the function of screw speed, screw geometry, and blend ratio.

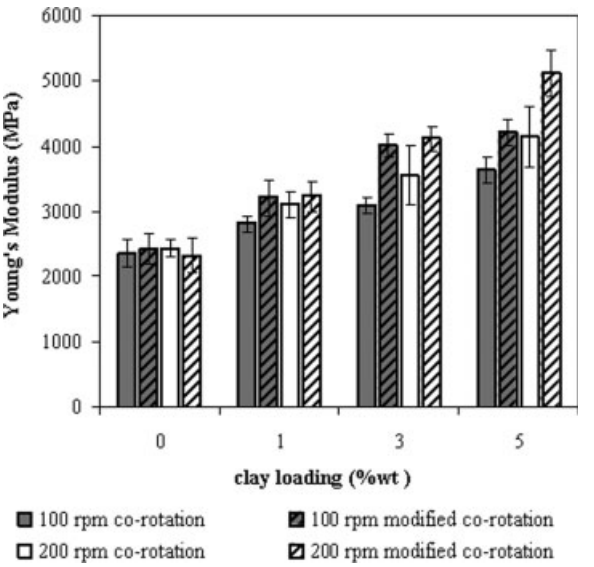

Figure 13 Young's Modulus of 50/50 blend based nanocomposites as the function of screw speed, screw rotation mode, and clay loading.

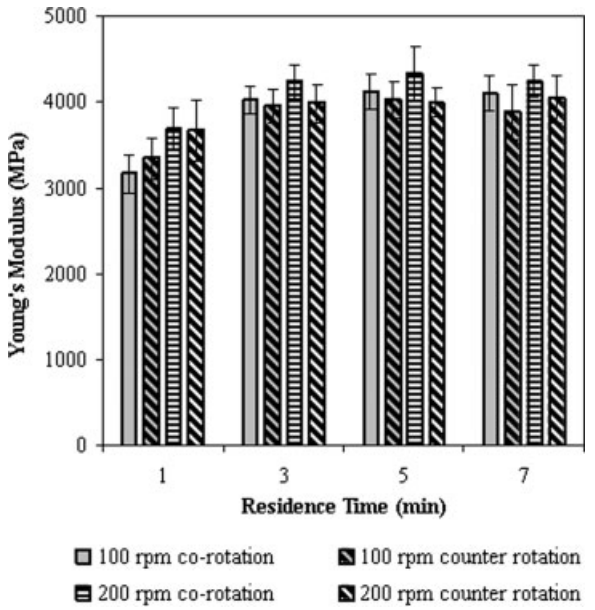

Figure 14 Young's Modulus of nanocomposites as the function of screw speed, screw geometry, and residence time for 5% clay reinforced 50/50 blend.

flow which is known to be effective in obtaining dispersive mixing.[18,50,51] In the current study, the effects of screw modification and screw speed on the modulus of 50/50/5 blend based nanocomposites are not significant at 1% clay loading level (see Fig. 13). Modification of the screws results in an increase in modulus of 3 and 5% clay containing nanocomposites at given screw speeds. Increasing screw speed also improves the modulus of the nanocomposite at 3 and 5% clay loading level. This improvement is so significant at 5% clay loading for the modified screws.

The residence times for laboratory mixing systems (i.e., batch extruders, internal mixers) are much longer as reported in the literature than that of in the current study;[12,13] however, in commercial systems, the average residence times are shorter. To examine the effect of residence time (1, 3, 5, and 7 min) on the modulus data as the function of screw speed, screw geometry of 50/50 blend based nanocomposites for the current mixing system are evaluated (see Fig. 14). It is observed that increasing residence time from 1 to 3 min yields an increase in modulus for given screw speed and screw rotation mode. Despite further increase in residence time, there is not any significant influence on the modulus.

CONCLUSIONS

The most important conclusions that can be drawn from the results of this study are:

i. Microcompounding conditions have great influence on blend morphology. In the case of dispersed phase morphologies (i.e. 80/20/5 and 20/80/5), the average size of the dispersed phase is smaller in nanocomposites processed with corotation rather than counter-rotation. For the nanocomposite based on 50/50/5, the cocontinuous morphology in corotation mode is disturbed in counter-rotation yielding a mixture of nonspherical dispersed particles in cocontinuous ABS/PA6.
ii. The exfoliation of the organoclays is enhanced with increasing PA6 in the matrix. Neat-ABS based nanocomposites exhibits intercalated nanomorphology. Increasing screw speed and mixing in corotation and modified corotation mode promotes the dispersibility of the clays.
iii. Organoclays are selectively localized in PA6 phase.
iv. The melt viscosity of the nanocomposites revealed from axial force measurements is inversely proportional to the PA6 composition in the blend. The reduction in axial force in modified corotation with respect to unmodified corotation is an indication of enhanced backflow at a given nanocomposite system and processing condition.
v. Incorporation of organoclay improves the modulus of the blends substantially. Increasing PA6 content and increasing screw speed raised the modulus of the nanocomposites. Screw modification is remarkably effective on modulus at higher clay loadings.

References

1. Vaia, R. A.; Ishii, H.; Giannelis, E. P. Chem Mater 1993, 5, 1694.
2. Vaia, R. A.; Jandt, K. D.; Kramer, E. J.; Giannelis, E. P. Macromolecules 1995, 28, 8080.
3. Dennis, H. R.; Hunter, D. L.; Chang, D.; Kim, S.; White, J. L.; Cho, J. W.; Paul, D. R. Polymer 2001, 42, 9513.
4. Lertwimolnun, W.; Vergness, B. Polym Eng Sci 2006, 46, 314.
5. Lertwimolnun, W.; Vergness, B. Polymer 2005, 46, 3462.
6. Li, X.; Park, H. M.; Lee, J. O.; Ha, C. S. Polym Eng Sci 2002, 42, 2156.
7. Quaedflieg, M.; Rijks, L. www.xplore-together.com/data/xplore_internet_paper.pdf, 2006.
8. www.xplore-together.com/home.htm, 2006.
9. Tiesnitsch, J. SPE ANTEC 2005, 6, 9.
10. Walia, P.; Barger, M.; Mc Kelvy, M. SPE ANTEC 2005, 1, 252.
11. Wroczynski, R. J.; Potyrailo, R. A.; Rubinsztajn, M. SPE ANTEC 2003, 3, 2679.
12. Stretz, H. A.; Paul, D. R. Polymer 2006, 47, 8527.
13. Pötschke, P.; Kretzschmar, B.; Janke, A. Compos Sci Technol 2006, 67, 855.
14. Maric, M.; Macosko, C. W. Polym Eng Sci 2001, 41, 118.
15. Breuer, O.; Sundararaj, U.; Toogood, R. W. Polym Eng Sci 2004, 44, 868.
16. Covas, J. A.; Costa, P. Polym Test 2004, 23, 763.
17. Yamaoka, I. Polymer 1998, 39, 1765.

18. Rauwendaal, C. Polymer Extrusion; Hanser Publisher: Munich, 2001.
19. Kitayama, N.; Keskkula, H.; Paul, D. R. Polymer 2001, 42, 3751.
20. Kitayama, N.; Keskkula, H.; Paul, D. R. Polymer 2000, 41, 8041.
21. Kudva, R. A.; Keskkula, H.; Paul, D. R. Polymer 2000, 41, 225.
22. Kudva, R. A.; Keskkula, H.; Paul, D. R. Polymer 1998, 39, 2447.
23. Majumdar, B.; Keskkula, H.; Paul, D. R. Polymer 1994, 35, 3164.
24. Majumdar, B.; Keskkula, H.; Paul, D. R. Polymer 1994, 35, 5453.
25. Kim, B. K.; Jeong, Y. M. L. H. M. Polymer 1993, 34, 2075.
26. Ozkoc, G.; Bayram, G.; Bayramli, E. J Appl Polym Sci 2007, 104, 926.
27. Ozkoc, G.; Bayram, G.; Bayramli E. SPE ANTEC 2006, 2, 650.
28. Rauwendaal, C.; Osswald, T.; Graman, P.; Davis, B. SPE ANTEC 1998, 1, 277.
29. Rauwendaal, C.; Anderson, J.; Del Pilar Noriega, M. Plast Eng 1997, 53, 41.
30. Rauwendaal, C.; Osswald, T.; Graman, P.; Davis, B. Int Polym Process 1999, 13, 28.
31. Fornes, T. D.; Paul, D. R. Polymer 2003, 44, 4993.
32. Taylor, G. I. Proc R Soc Lond Ser A 1932, 138, 41.
33. Taylor, G. I. Proc R Soc Lond Ser A 1934, 146, 501.
34. Paul, D. R.; Bucknall, C. B. Polymer Blends; Wiley: New York, 2000.
35. Hettema, R.; Tol, J. V.; Janssen, L. P. B. M. Polym Eng Sci 1999, 39, 1628.
36. Homminga, D.; Goderis, B.; Hoffman, S.; Reynaers, H.; Groeninckx, G. Polymer 2005, 46, 9941.
37. Ahn, C. Y.; Paul, D. R. Polymer 2006, 47, 2830.
38. Li, Y.; Shimizu, H. Macromol Rapid Commun 2005, 26, 710.
39. Chiu, F. C.; Lai, S. M.; Chen, Y. L.; Lee, T. H. Polymer 2005, 46, 11600.
40. Li, L.; Bellan, L. M.; Craighead, H. G.; Frey, M. W. Polymer 2006, 47, 6208.
41. Gonzalez, J.; Eguiazabal, I.; Nazabal, J. Eur Polym J 2006, 42, 2905.
42. Gonzalez, J.; Eguiazabal, I.; Nazabal, J. Compos Sci Technol 2006, 66, 1833.
43. Chavarria, F.; Paul, D. R. Polymer 2006, 47, 7760.
44. Lee, H. S.; Fasulo, P. D.; Rodgers, W. R.; Paul, D. R. 2005, 46, 11673.
45. Chavarria, F.; Paul, D. R. Polymer 2004, 45, 8501.
46. Gatos, K. G.; Martínez Alcázar, J. G.; Psarras, G. C.; Thomann, R.; Karger-Kocsis, J. Compos Sci Technol 2006, 67, 157.
47. Lewis, T. B.; Nielsen, L. E. J Appl Polym Sci 1970, 14, 1449.
48. Nielsen, L. E.; Landel, R. F. Mechanical Properties of Polymers and Composites: Marcel Dekker: New York, 1994.
49. Cho, J. W.; Paul, D. R. Polymer 2001, 42, 1083.
50. Manaz-Zloczower, I.; Tadmor, Z. Mixing and Compounding of Polymers; Hanser Publisher: Munich, 1994.
51. Utracki, L. A. Two Phase Polymer Systems; Hanser Publisher: Munich, 1991.